3rd URSI AT-AP-RASC, Gran Canaria, 29 May – 3 June 2022

Detection and localization of shallow buried targets: experimental results

A. Brancaccio*(1), G. Leone(1) and R. Solimene(1)
(1) Università della Campania - Dipartimento di Ingegneria, Italy, Aversa, 81031, www.unicampania.it

Abstract

Experimental results concerning the detection and localization of shallow buried targets are shown. The imaging method relies on a convenient two dimensional mathematical formulation, in which the third spatial dimension, that is the depth, is neglected. The input data are bistatic measurements, where the source is fixed and the receiving antenna moves onto a plane parallel to the air/ground interface. Each set of spatial measurements is taken at one single frequency. The use of several sets, taken at different frequencies, allows to perform detection and localization with few (undersampled) spatial data.

1 Introduction

In ground penetrating radar (GPR) applications there is a growing interest in achieving target detection through non-contact measurement layouts, for example, with GPRs mounted on a flying platform [1, 2]. This configuration allows to inspect electrically large spatial regions even if the area is not easily acessible otherwise. In this framework, the large the number of measurements to be managed on board from one side, and the need to syncronize receviers and transmitters from the other side, may constitute technical limitations [3]. In order to counteract such drawbacks, we have recently introduced a microwave imaging algorithm that looks for the scattering targets in terms of equivalent surface currents supported over a given reference plane [4]. While this method is suited to detect shallowly buried targets, it allows one to independently process all frequency data, and hence the source and the receivers do not need to be synchronized. Moreover, spatial data can be reduced to a large extent, without any aliasing artifacts, by properly combining single-frequency reconstructions [5, 6]. Here, we report some experimental results that show the feasibility of the method. In particular, the experimental test site consists of a sand box in open air where a metallic plate is shallowly buried (at few centimetres) under the air/soil interface. The investigated region is illuminated by a fixed transmitting horn antenna, whereas the scattered field is collected over a planar measurement aperture at a fixed height from the air-sand interface (see Figure 1). The transmitter and the receiver share only the working frequency information.

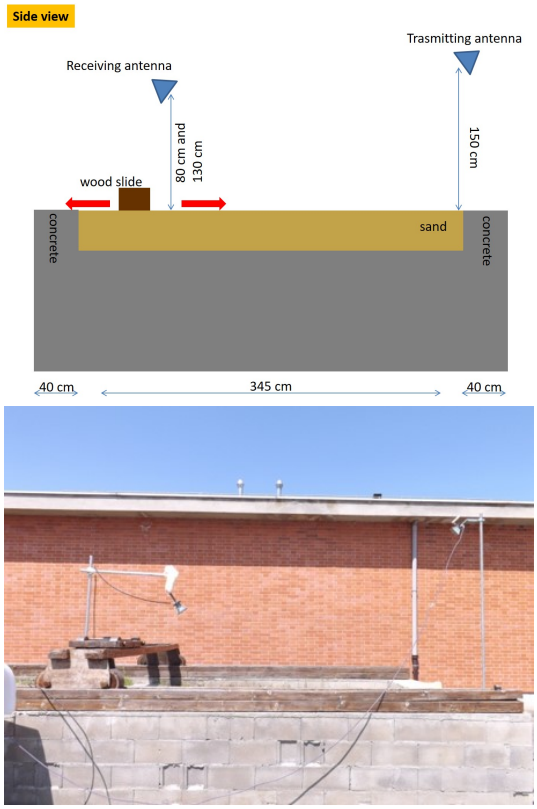

Figure 1. Schematic side view of the measurement configuration (top) and photo of the test site (bottom).

2 Method

A detailed derivation of the model can be found in [5, 6], here we outline only the basic steps. We consider a two-layered background medium with the upper half-space being air, while the lower one models the soil. A cartesian reference system with vertical z-axis is considered where the air/soil interface is located at $z = 0$. The targets are located in the lower half-space (i.e., for $z < 0$), buried in close proximity to the separation interface. We look for the targets inside a 2D investigation domain denoted as $D = [-x_M, x_M] \times [-y_M, y_M]$ at the fixed depth z_T. The scattering scene is probed by a single source located in the upper half-space at some stand-off distance from the air/soil interface. The field scattered by the buried targets is collected over a set of positions still located on the air side and all at the same height h_O. By invoking the equivalence theorem [7], the scattered field can be considered as being

radiated by equivalent surface magnetic currents supported over the plane $z = z_T$. Each cartesian component of such an equivalent current is represented as

$$J_{eq}(x,y;k_l) = \sum_{n=-N}^{N} \sum_{m=-M}^{M} I_{mn} \exp\left[-j\pi\left(\frac{mx}{x_M} + \frac{ny}{y_M}\right)\right]. \quad (1)$$

where I_{nm} are the Fourier coefficients at the l-th frequency k_l and the exponentials represent the two-dimensional Fourier spatial harmonics in the domain of investigation. The support of such current denotes the presence of targets. It can be shown that the voltage measured at each receiver location is linearly related to the (unknown) current distribution by an operator taking into account the receiving antenna response. After passages that we skip here for brevity, we arrive at the discretized model

$$\mathbf{V}(k_l) = \mathbf{H} \cdot \mathbf{I}, \quad (2)$$

where $\mathbf{V}(k_l) \in C^{N_O}$ is the data vector, that is the voltage measured at N_O locationd inside D, $\mathbf{H} \in C^{N_O \times (2N+1)(2M+1)}$ is the matrix version of the scattering operator (whose computation requires the knowledge of the frequency, of the measurement point locations, of the antenna response in terms of gain and polarization, but *not* of the source location), and $\mathbf{I} \in C^{(2N+1)(2M+1)}$ is the (vectorized) matrix of the Fourier coefficients I_{mn} of the current. Accordingly, the unknowns of the problem now become the expansion coefficients I_{nm}. The choice of N and M is linked to the so-called number of degrees of freedom of the problem, reflects the ill-posedness of the inverse problem at hand, and depends on the operating frequency as well as on the investigation and the observation domain extensions [4, 5].
Equation (2) is inverted for $\mathbf{I}$ by a standard Truncated Singular Value Decomposition (TSVD) [8] of the relevant matrix operator. This allows to counteract the ill-posedness of the problem and to obtain a stable reconstruction. Once the coefficients I_{nm} have been recovered, the corresponding equivalent current $J_{eq}(x,y;k_l)$ is computed by means of (1). Then, the support of such an equivalent surface current is provided by the image in the x,y investigation domain,

$$I(x,y;k_l) = |J_{eq}(x,y;k_l)|. \quad (3)$$

In order to limit the system complexity, the number of spatial data must be reduced. This in general can lead to a reconstruction that is corrupted by aliasing artifacts that are difficult to distinguish from the actual current. To cope with this drawback, a simple strategy based on the combination of single-frequency reconstructions has been introduced in [5]. In more detail, suppose that N_k is the number of adopted frequencies; then the final reconstruction is obtained as

$$I(x,y) = \Pi_{l=1}^{N_k} I(x,y;k_l). \quad (4)$$

The very basic idea behind (4) is that aliasing artifacts change positions with the working frequency, whereas the actual source reconstruction does not. Therefore, (4) tends to mitigate all those peaks in the reconstruction that do not overlap (or overlap only partially) while the frequency changes. A criterion for the choice of the frequencies is provided in [5]. In sum, the algorithm presents the following steps:
1. fix one frequency value;
2. compute the scattering matrix model $\mathbf{H}$;
3. compute the SVD of $\mathbf{H}$;
4. fix a regularizing threshold for the normalized singular values of $\mathbf{H}$ (in the following experimental results, 20dB is used) and compute the unknown vector $\mathbf{I}$ via a TSVD inversion by retaining the data projection over the singular vectors corresponding to the singular values above the threshold;
5. calculate $I(x,y;k_l)$ by (1) and (3);
6. repeat from step 1 to step 5 by changing the frequency value;
7. compute $I(x,y)$ from (4).

3 Experimental Results

The test site consisted of a tank full of sand of about 3.5 m (length) 2.5 m (width) and 1.5 m (depth) in size. The tank was placed in the open air so that the sand appeared wet, apart from the very surface layer, which was dried by sun. The electromagnetic features of the sand were unknown and were not estimated (as they are not needed for detection purposes).
The transmitting antenna was a horn positioned at a $h_t = 1.5$ m height from the sand floor and located at one of the end sides of the tank. It was tilted to point to the spatial region under investigation. The receiving antenna was still a horn and was located on the other side of the tank. In particular, it was mounted on a wooden slide that allowed it to synthesize a planar measurement aperture at a fixed height h_O from the air/sand interface. The receiving antenna was tilted toward the investigated spatial region and was linearly polarized. Figure 1 shows a schematic view of the measurement configuration along with a picture of the test site. A metallic rectangular plate 17.5 cm $\times$ 48 cm in size was used as target. A vector network analyzer was connected to the antennas by means of coaxial cables. Standard calibration at the end of each channel was performed at the beginning of each measurement stage in order to avoid mismatch between VNA and cables.
The investigation domain is a rectangle of 160 cm along the x and 100 cm along the y direction, and it is located at $z_T = 0$. We also introduce the two parameters *offsetx* and *offsety*, which indicate the displacement, along the x and y directions, respectively, of the center of the investigation domain with respect to the central point of the first measurement line (see Figure 2 for the reference system). Basically, after acquiring the data, changing the investigation domain center location (by varying the offset parameters) entails looking for the targets in different spatial regions. Accordingly, the same target will appear at different relative positions. This can be considered as a way to check reconstructions' consistency and stability. A detection can be considered successful if the target localization point moves coherently with the displacement of the investigation do-

main center.

For the example below, we collected data over a grid of 8×7 positions. To this end, the receiving antenna scanned the measurement aperture with a spatial step (along both the x and y directions) of 20 cm and $h_O = 130$ cm. The spatial data are under-sampled, and to overcome aliasing we processed data collected at $N_k = 11$ frequencies within the band [2–4] GHz, in order to be as close as possible to frequency selection criterion provided in [5]. In Figure 3

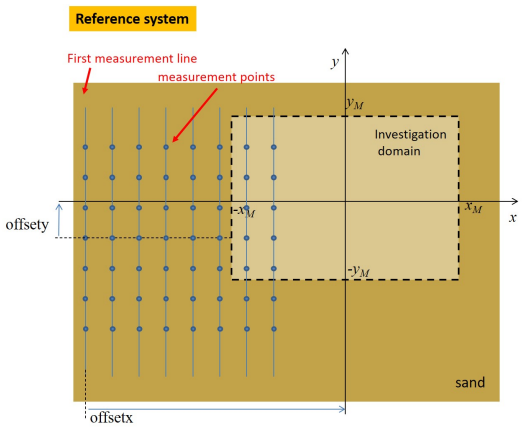

Figure 2. Investigation domain and measurement points; the reference system is centred on the investigation domain.

we show the reconstruction of a shallowly buried target obtained by employing all the available frequencies. As can be appreciated, the target is clearly detected and the related hot spot indicator changes position accordingly to the investigation domain center offset. In rder to appreciate the role of the reflection from the ground in Figure 4 we report the reconstructions obtained by processing background data, i.e., data collected in absence of the target. Differently from the target case, now the reconstructions do not exhibit a clear hot spot. Moreover, the reconstruction changes as the investigation domain center offset varies. This entails that processing air/soil interface reflection does not return a focused hot spot. Furthermore, the reconstruction corresponding to this contribution is in general different when the investigated spatial region changes. Eventually, these results suggest a possible strategy to recognize actual targets against surface clutter. Indeed, comparing images obtained using different investigation domain offsets, the actual targets are those ones for which the reconstructions "move" coherently with the change in the investigation domain center.

In Figure 5 the investigation domain is kept fixed with *offsetx* = 2.0 m, *offsety* = 0.3 m and different number of frequencies N_k are employed. As can be seen, when N_k increases, the aliasing artifacts actually tend to disappear and the hot spots narrows. This is, of course, expected and perfectly consistent with the theoretical arguments discussed in [5].

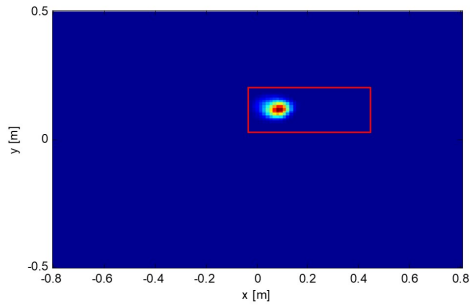

offsetx = 1.7 m, *offsety* = 0.0 m

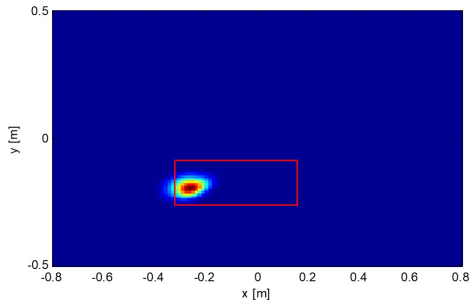

offsetx = 2.0 m, *offsety* = 0.3 m

Figure 3. Normalized reconstructions of a shallowly buried target for two different investigation domain offsets. The actual target location is indicated by the red rectangle.

4 Acknowledgements

This research was partially funded by VALERE: VAnviteLli pEr la RicErca research program by Universita degli Studi della Campania Luigi Vanvitelli.

References

[1] I. Catapano, L. Crocco, Y. Krellmann, G. Triltzsch, F. Soldovieri,"A Tomographic Approach for Helicopter-Borne Ground Penetrating Radar Imaging," *IEEE Geosci. Remote Sens. Lett.*, 2012, **9**, pp. 378–382, doi:10.1109/LGRS.2011.2169390.

[2] M.G. Fernández, Y.Á López, A.A. Arboleya, B.G. Valdés, Y.R. Vaqueiro, F.L.H. Andrés, A.P. García, "Synthetic aperture radar imaging system for landmine detection using a ground penetrating radar onboard an unmanned aerial vehicle," *IEEE Access*,2018, 6, pp. 45100–45112, doi:10.1109/ACCESS.2018.2863572.

[3] I. Catapano, G. Gennarelli, G. Ludeno, C. Noviello, G. Esposito, F. Soldovieri, "Contactless Ground Penetrating Radar Imaging: State of the Art, Challenges, and Microwave Tomography-Based Data Pro-

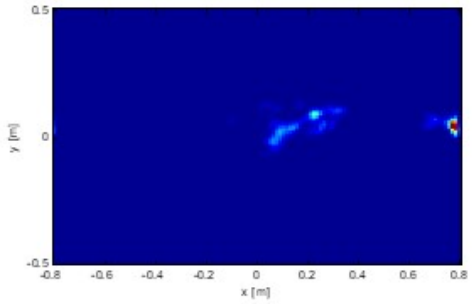

offsetx = 1.7 m, *offsety* = 0.0 m

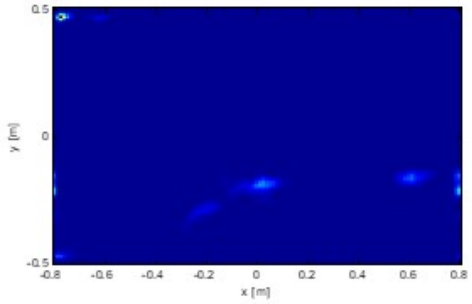

offsetx = 2.0 m, *offsety* = 0.3 m

Figure 4. Normalized reconstructions by data collected in absence of target.

cessing," *IEEE Geosci. Remote Sens. Mag.*, 2021, doi:10.1109/MGRS.2021.3082170.

[4] A. Brancaccio, G. Leone, R. Solimene, "Single-frequency Subsurface Remote Sensing via a Non-Cooperative Source," *J. Electrom. Waves Appl.*, 2016, 30, pp. 1147–1161, doi:10.1080/09205071.2016.1182086.

[5] A. Brancaccio, A. Dell'Aversano, G. Leone, R. Solimene, "Subsurface Detection of Shallow Targets by Undersampled Multifrequency Data and a Non-Cooperative Source," *Appl. Sci.*, 2019, 9, pp. 5383, doi:10.3390/app9245383.

[6] A. Brancaccio, G. Leone, R. Pierri and R. Solimene, "Experimental Validation of a Microwave Imaging Method for Shallow Buried Target Detection by Under-Sampled Data and Non-Cooperative Suorce," *Sensors*, 2021, 1, 0, doi:10.3390/s1010000.

[7] C. Balanis, *Advanced Engineering Electromagnetics*; Wiley and Sons: New York, NY, USA, 1989.

[8] M. Bertero M. and P. Boccacci, *Introduction to Inverse Problems in Imaging*, Institute of Physics: Bristol, UK, 1998; ISBN 9780750304351.

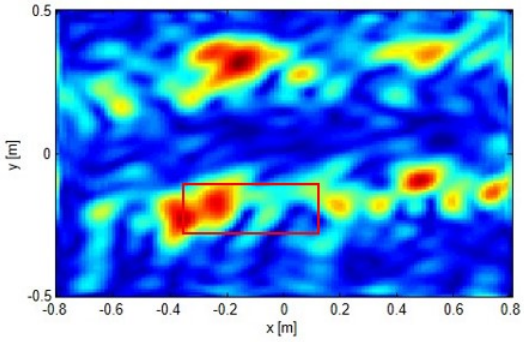

$N_k = 1$

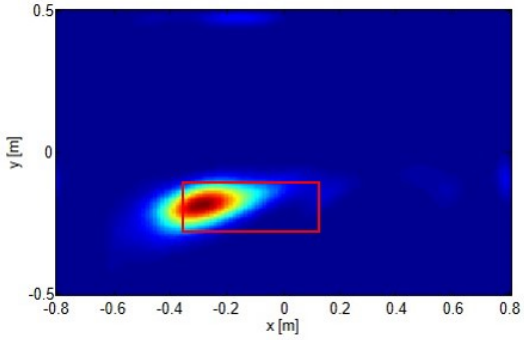

$N_k = 3$

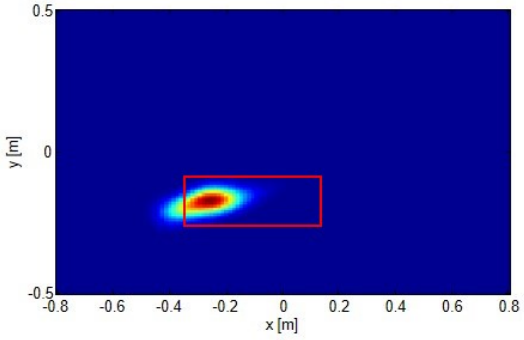

$N_k = 5$

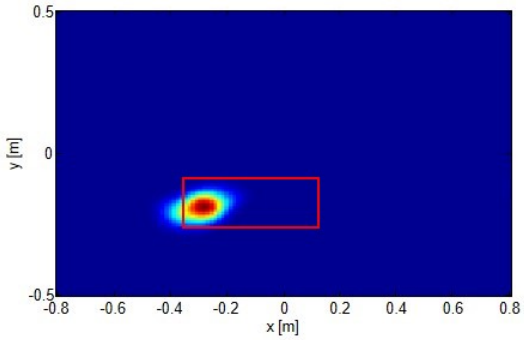

$N_k = 7$

Figure 5. Comparison of reconstructions obtained by employing different number of frequencies N_k. The actual target location is indicated by the red rectangle.